Ann. Geophys., 28, 1221–1228, 2010
www.ann-geophys.net/28/1221/2010/
doi:10.5194/angeo-28-1221-2010

Annales Geophysicae

3-D-geocoronal hydrogen density derived from TWINS Ly-α-data

J. H. Zoennchen, U. Nass, G. Lay, and H. J. Fahr

Argelander Institut für Astronomie, Astrophysics Department, University of Bonn, Auf dem Huegel 71, 53121 Bonn, Germany

Received: 23 February 2010 – Revised: 17 May 2010 – Accepted: 20 May 2010 – Published: 1 June 2010

Abstract. Based on Ly-α-line-of-sight measurements taken with two Ly-α detectors onboard of the satellite TWINS1 (Two Wide-angle Imaging Neutral-atom Spectrometers) density profiles of the exospheric, neutral geocoronal hydrogen were derived for the time period between summer solstice and fall equinox 2008. With the help of specifically developed inversion programs from Ly-α line of sight intensities the three-dimensional density structure of the geocoronal hydrogen at geocentric distances $r > 3\,R_E$ could be derived for the period mentioned characterized by very low solar 10.7 cm radiofluxes of ≈65–70 [10^{-22}W m^{-2} Hz^{-1}]. The time-variable, solar "line-centered"-Ly-α-flux was extracted on the basis of daily (terrestrial) NGDC 10.7 cm radioflux data using the models from Barth et al. (1990) and Vidal-Madjar (1975).

The results for the geocoronal H-densities are compared here both with theoretical calculations based on a Monte-Carlo model by Hodges (1994) and with density profiles obtained with the Geocoronal Imager (GEO) by Østgaard and Mende (2003). In our results we find a remarkably more pronounced day-/night-side asymmetry which clearly hints to the existence of a hydrogen geotail (i.e. a tail structure with comparatively higher hydrogen densities on the night side of the earth for geocenctric distances $>4\,R_E$), and a only weakly pronounced polar depletion. These unexpected features we try to explain by new models in the near future. The derived 3-D-H-density structures are able to explain the line-of-sight (LOS) dependent Ly-α intensity variations for all LOS seen up to now with TWINS-LAD. The presented results are valid for the region with geocentric distances $3\,R_E < r < 7\,R_E$ and are based on the reasonable assumption of an optically thin H-exosphere with respect to resonant Ly-α-scattering allowing the use of single scattering calculations.

Correspondence to: J. H. Zoennchen
(zoenn@astro.uni-bonn.de)

Keywords. Atmospheric composition and structure (Airglow and aurora; Pressure, density, and temperature) – Meteorology and atmospheric dynamics (Thermospheric dynamics)

1 Introduction

The outermost region of the earth's atmosphere, the geocorona, is dominated by neutral hydrogen as the representative atmospheric gas constituent. Geocoronal hydrogen is resonantly excited by the solar Ly-α-emission and thus leads to a diffuse Ly-α resonance glow radiation pattern. This easily observable, intense geocoronal UV radiation contains singular informations on the global structure and dynamics of the neutral hydrogen density since local radiation sources are proportional to local hydrogen properties like H-density and H-temperature. For geocentric distances $r > 3\,R_E$ the H-densities are low enough to allow the assumption of optically thin conditions. Thus single scattering approaches are justified for the calculation of the Ly-α resonant radiation field. In case of single scattering the locally scattered Ly-α radiation is proportional to the local H-density and the LOS intensity is proportional to the LOS H-column density. The two TWINS-satellites are on highly elliptical Molnija orbits. On their trajectories TWINS satellites, besides two imaging ENA cameras (see McComas et al., 2009) carry with them two Ly-α detectors which register the geocoronal Ly-α radiation at geocentric distances of between 1.5 and 7 R_E from different orbital vantage points and associated LOS-directions. From the deconvolution of these LOS measurements based on a three-dimensional H-density model of the hydrogen geocorona the 3-D-density structure as well as its dynamics can be derived for geocentric distances $r > 3\,R_E$.

Published by Copernicus Publications on behalf of the European Geosciences Union.

2 TWINS-LAD-instrumentation, data-cleaning

2.1 The TWINS Ly-α-detector (LAD)

Each of the TWINS satellites is equipped with 2 independently operated Ly-α-detectors (LADs) which are mounted with a tilt angle of 40° with respect to the spin axis of the actuator platform (TWA) rotating the instrument in a windshield wiper mode by 180 degrees. The spin axis of the TWA is actively aligned with the direction towards the earth's center by spacecraft manoeuvres during the whole mission. With an aperture of $4° \times 4°$ each LAD-detector counts resonantly scattered geocoronal Ly- α-photons. The wavelengths of the countable photons is narrowed to ± 50 Å around the Ly-α center line by the use of resonant interference filters. The scanning process for a full circle takes about 60 s. All LAD-detectors were absolutely calibrated at the BESSY-Synchrotron in Berlin before mission start (see Richter et al., 2001, for the procedure). More detailed informations concerning the instrumentation and the mission program of the TWINS satellites are published in Nass et al. (2006) and McComas et al. (2009).

2.2 Data cleaning

Since the observed radiation originates from the optically thin regime for geocoronal Ly-α glow the radiation transport theory allows for the single scattering approximation. In order to achieve this assumption all lines of sight passing through earth impact altitudes closer than geocentric distances of 3 R_E are thus removed. In addition all LOS with a passage through the earth's shadow, approximated by a cylinder with the radius of 1 R_E in the antisolar direction, are removed as well. Altogether only those LAD-data taken under acceptably correct operation conditions (particularly with respect to the actual high voltage for both instruments) are used in our analysis. In order to avoid disturbances caused by contaminations like indirectly (presumably instrumental) backscattered solar UV light all LOS with angles to the sun smaller than $< 85°$ are removed. Possible stigmatic small-angle point emissions caused by Ly-α bright stars are mostly negligible after using an angle-averaging procedure for each LOS with nearby lines of sight.

2.3 Albedo correction

The resonant scattering process and the radiation transport is not only connected with Ly-α photons entering the atmosphere directly from the sun (i.e. the direct solar Ly-α radiation component) but in addition also influenced by Ly-α photons with an origin in the lower optically thick atmospheric regions of the earth. The effect of that radiation contribution can be well estimated (see Zoennchen, 2006) and for geocentric distances larger than 3 R_E is smaller than 2% as compared with the resonance glow intensity caused by scattering of the direct solar Ly-α radiation and even decreases with altitude quadratically. For the quiet and very stable solar conditions prevailing during the analysed time period an integrated solar line intensity of 35 kR is reradiated from the lower H-geocorona ($\approx$700 km altitude) (see also Østgaard and Mende, 2003).

2.4 Contribution from transcharged fast solar H-atoms

The pristine supersonic solar wind is only met by geocoronal H-atoms in the region outside the terrestrial magnetobow shock (i.e. $d \geq 10\,R_E$). Here in fact H-atoms originate from charge exchange with the solar wind protons that move antisolar with velocities of the order of $v_s \simeq 400$ km/s. They in principle can be resonantly excited by the solar Ly-α emission at spectral regions offplaced from the line center by $\Delta\lambda_s = \lambda_0 \cdot (v_s/c) \simeq 1.6$ Å with spectral intensities lower by a factor $g_s \simeq I_0 \cdot \exp[-(\Delta\lambda_s/\Delta\lambda_0)^2]/I_c \simeq 10^{-3}$ where the halfwidth of the solar Ly-α line has been adopted with $\Delta\lambda_0 = 0.6$ Å and the linecenter depletion with $I_c = 0.8 \cdot I_0$. This means that these solar wind-type H-atoms are resonantly excited with g-factors smaller by about 10^{-3} compared to geocoronal H-atoms which on all lines of sight used by us also have much higher densities. The contribution of this effect is therefore negligible.

3 Solar conditions and interstellar Ly-α-background

3.1 Solar Ly-α line centered flux

In the relevant time period from June to August 2008 exceptionally quiet, nearly temporally constant solar activity conditions at a very low activity level were prevailing. The 10.7 cm radioflux as an index for the solar activity fluctuated only by about $\pm 2.5\%$ around an average value of $\approx 68\,[10^{-22}\mathrm{W\,m^{-2}\,Hz^{-1}}]$ in the mentioned time period (see Fig. 1).

The total, solar Ly-α-flux is correlated with the solar 10.7 cm radioflux (see Barth et al., 1990). Between the total, solar Ly-α-flux and the line centered, solar Ly-α-flux there exists a quasi-linear correlation as published by Vidal-Madjar (1975). Both correlations were used to calculate the relevant Ly-α-photon flux of solar Ly-α center photons with a value of 2×10^{11} photons $\mathrm{cm^{-2}\,s^{-1}\,Å^{-1}}$. Daily variations of the averaged solar Ly-α-radiation input were in the range of less than $\pm 3\%$.

3.2 Ly-α-background radiation from the interstellar medium

The resonant Ly-α intensity originating at interplanetary hydrogen atoms streaming into the solar system from the local interstellar medium (LISM) needs to be treated separately with available theoretical models (e.g. Bzowski et al., 2003) and needs to be removed as an additional radiation contribution. Intensities of this interplanetary glow are strongly

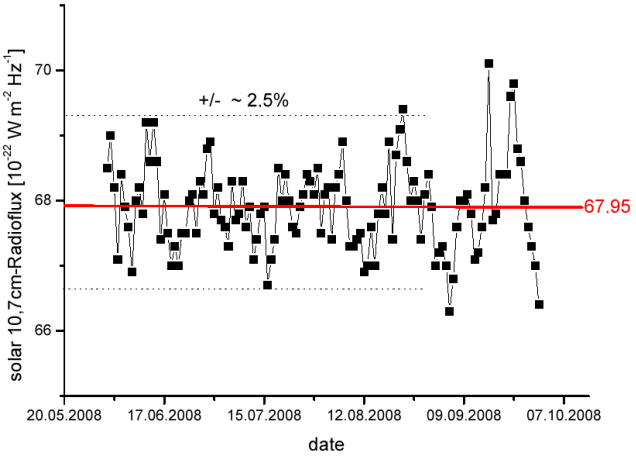

Fig. 1. Shown are very small variations of the solar 10.7 cm radioflux (daily measured from NGDC, Ottawa, Canada) from June to August 2008 with an average value of ≈67.95 ± 2.5% indicating a stable averaged solar Ly-α-radiation input.

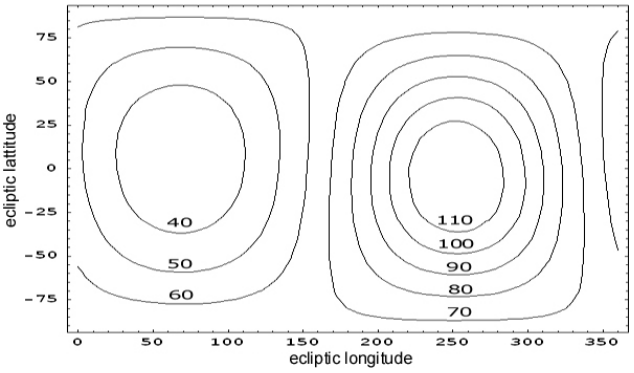

Fig. 2. Calculated interplanetary Ly-α-background intensity map in Rayleigh for 11 June 2008 based on the model by Wu and Judge (1979) with $n_{\mathrm{H,LISM}} = 0.1\,\mathrm{cm}^{-3}$, 10.7 cm radioflux=68 $[10^{-22}\mathrm{W\,m^{-2}\,Hz^{-1}}]$.

varying with ecliptic view directions and with the phase of the solar activity cycle (see Fahr, 2004, for a recent review). Solar Ly-α-radiation is resonantly scattered by the LISM-atoms in the ambient interplanetary space and represents a TWINS-LAD observable Ly-α-radiation background which is temporally varying with the solar activity cycle in its intensity distribution.

Based on a "hot model" published by Wu and Judge (1979) (see also Pryor et al., 2008) different Ly-α-background maps for all analysed days were calculated and then subtracted from their respective LAD-measurements (see Fig. 2). With values ranging up to some 10^2 R the interplanetary Ly-α-background only becomes quantitatively comparable with geocoronal resonant scattering intensities in the outermost geocorona. The TWINS1-LAD measurements presented in this paper with geocentric distances up to 6 R_{E} contain fractions of the interplanetary Ly-α-background radiation limited to less than 10–15%, but staying in the range of only 2–5%.

4 First approximation: spheric symmetric density

4.1 H-Density profiles

As a first and starting approximation, the neutral H-density of the actual geocorona was deconvoluted assuming a simple r-dependent exponential H-density distribution according to $\mathrm{y} = \mathrm{a} \cdot \exp(-\mathrm{r/b}) + \mathrm{c}$ for 3 different dates from June to August 2008. These exponential model fits already well the general altitude-dependence of the Ly-α-intensity and of the respective proportional H-LOS column density (see the red area of the model fit in Fig. 3a–c), but these fits do not explain the scatter in the measured data (as seen in the black area in Fig. 3).

This scatter is in fact a clear hint for additional angle-dependent H-density structures within the geocorona as discussed in the following sections. These ϕ- and θ-dependent densities cause different Ly-α-emissions for viewing points with the same altitude, but with different longitudes and latitudes of the LOS.

The comparison in Fig. 4 of the TWINS-derived H-density profiles both with the results by Østgaard and Mende (2003) and with the Solstice-model (10.7 cm radioflux = 80) by Hodges (1994) furthermore shows that the TWINS-derived H-density profiles decrease much slower with increasing altitude as compared to the measured/respectively predicted data published by the other mentioned authors. This could be an important hint to the existence of a so far underestimated population of long living H-atoms moving on satellite orbits above the exobase (see Chamberlain, 1963) and relevantly contributing to the H-densities in the outer exospheric region of the geocorona.

4.2 Depletion of neutral H-atoms over the northpole

In the polar geocoronal regions a remarkable depletion of the neutral H-densities in comparison with equatorial densities for equal altitudes is presently expected by models (see Hodges, 1994). The relevant loss of H-atoms is expected to be due to charge exchange processes of cold H-atoms with fast polar wind protons and was quantitatively predicted by the Hodges-model (1994).

To analyse this prediction with TWINS1-data two separate exponential fits were carried out: the first fit only used LOS which pass the earth over the north polar region ($75° \leq \theta \leq 90°$), while the second fit only includes LOS passing the earth in the equatorial (dayside) region ($-20° \leq \theta \leq 20°$, $\phi \approx 180°$). The result of these two separate exponential fits is shown in Fig. 5. As it turns out from this figure, there is no remarkably large difference in the general H-density profile and absolute density between polar LOS (black squares)

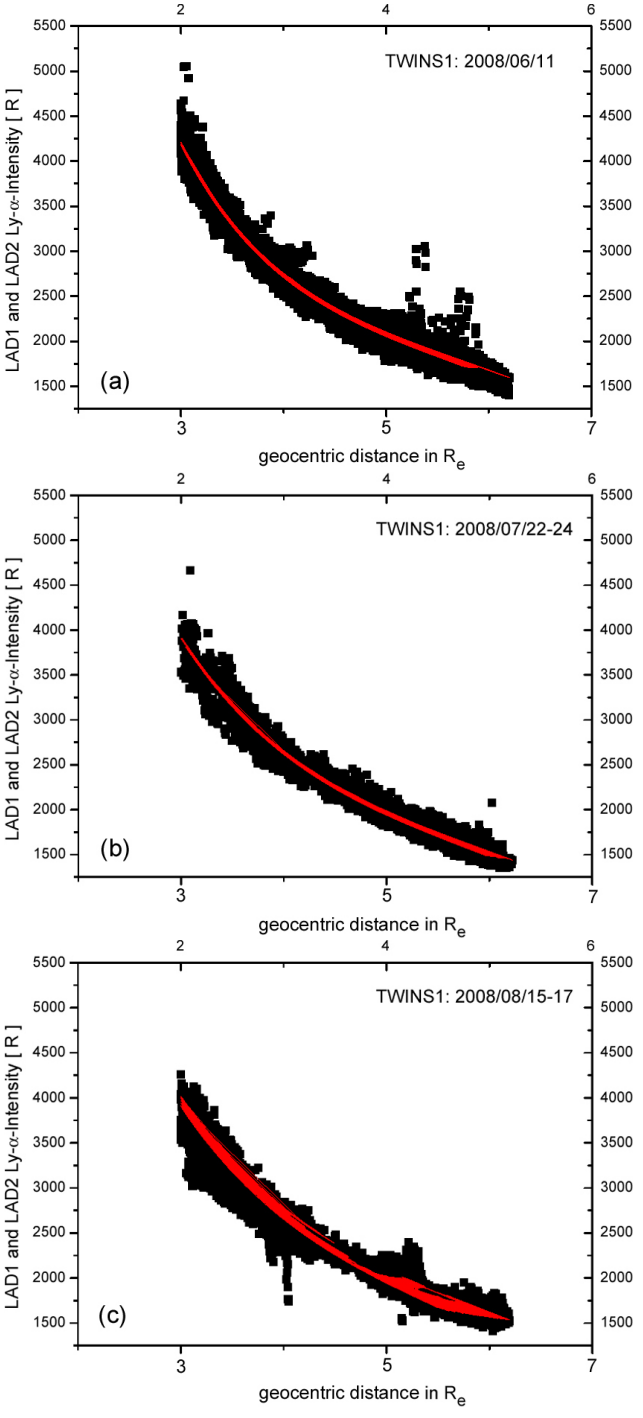

Fig. 3. Measured TWINS1 Ly-α-intensity profiles (black) in Rayleigh plotted versus the "line-of-sight" (LOS) earth passing geocentric distance in R_E for 11 June **(a)**, 22–24 July **(b)** and 15–17 August **(c)** in 2008. The red area is showing the calculated LOS-intensities based on the r-dependent H-density model which fits the general profile but could not explain the width of the intensity scatter within the profiles.

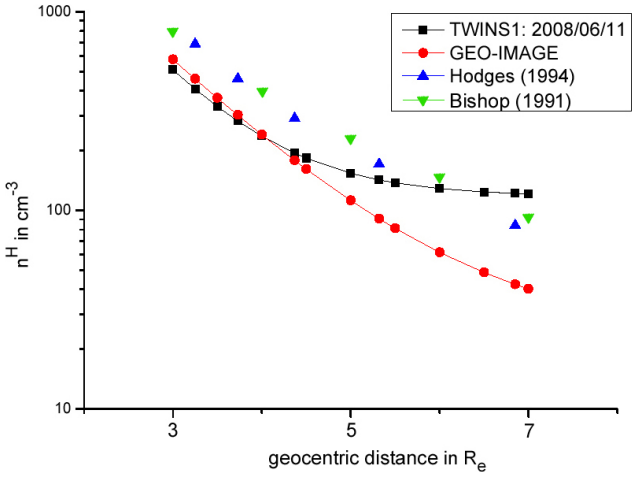

Fig. 4. Comparison of different H-density profiles: exponential model TWINS1 (black), H-density profile ($\phi = 90°$) by Østagaard and Mende (2003) (red), H-density profile ($\phi = 90°$) by Bishop (1991) (green) and averaged equatorial profile (Solstice, 10.7 cm radioflux=80) by Hodges (1994) (blue).

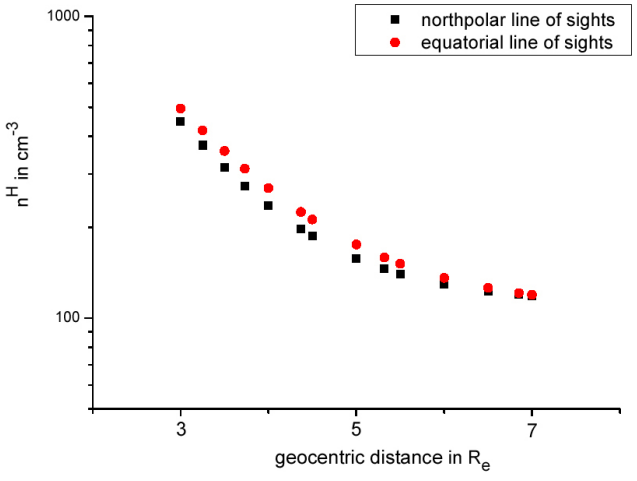

Fig. 5. Separately fitted H-density profiles (11 June 2008) for lines of sight with earth passing point in the north pole region (black) and in the equatorial region (red), respectively. The equatorial H-density profile is only slightly higher then the polar profile, that points to a weak pole/equator asymmetry.

and equatorial LOS (red circles) recognizable, the equatorial densities are only slightly higher than the polar densities. That means that the depletion of the neutral H-atoms over the northern pole compared to the H-atom densities in equatorial regions seems to be much less pronounced than predicted (seen by TWINS: ≈10–15%, Hodges(1994): from 25% up to 150% for larger distances). Reasons for that could be seen in a less effective charge exchange coupling to the polar wind (see Fahr et al., 2007) or a weaker polar wind as described by Holzer and Banks (1969).

The same analysis, however, done with fits by the 3-D-geocoronal H-density model as will be discussed in the following section of the paper also leads to very small H-density differences between polar and equatorial H-atom geocorona distributions.

5 3-D-density stucture

5.1 Coordinate system

For the 3-D deconvolution of the daily TWINS-data we used a sun aligned, earth centered, equatorial coordinate system (x,y-plane is within the earth equator, $\theta = 90°$ points to the earth's north pole) with $\phi = 0°$ pointing always to the midnight meridian in the antisolar direction. This coordinate system makes one complete circulation per year with respect to the earth centered equatorial coordinate frame (ECI) and points towards the sun.
Due to the mission profile (i.e. orbital geometry of the TWINS satellite) the TWINS-data contain LOS-measurements from the Northern Hemisphere only, the southern geocoronal region was not touched (observed) so far.

5.2 H-model description

As a mathematical model for the three-dimensional H-density fits we basically used a spheric harmonic representation

$$n_{\mathrm{H}}(r,\phi,\theta) = N(r)\sqrt{4\pi}\sum_{l=0}^{2}\sum_{m=0}^{l} Z(r,\phi,\theta) \quad (1)$$

with

$$Z = [A_{\mathrm{lm}}(r)\cos(m\phi) + B_{\mathrm{lm}}(r)\sin(m\phi)]Y_{\mathrm{lm}}(\theta) \quad (2)$$

and the spheric harmonic Legendre-polynomials $\mathrm{Y_{lm}}(\theta)$.

In order to reduce the large amount of coefficients to a reasonably fitable number we used a maximum number of $l = 2$ and neglegted all the $\mathrm{B_{lm}(r)}$-coefficients, because a sun-aligned, ϕ-symmetric structure for the H-geocorona can be assumed. For that reason a longitudinal sun-aligned coordinate system was chosen as described in the previous subsection.

Furthermore the in principle arbitrary r-dependences of N(r) and the $\mathrm{A_{lm}(r)}$-coefficients were replaced by simple, but reasonable functions which are fitted using the Hodges-model. To handle particularly the N(r)-term we used either a powerlaw $\mathrm{N(r) = a \cdot r^{-b}}$ or an exponential $\mathrm{y = a \cdot \exp(-r/b) +}$ c function.

Detailed information concerning the specially developed "Bonn-model" of the geocoronal H-density is published in Nass et al. (2006) and Zoennchen (2006).

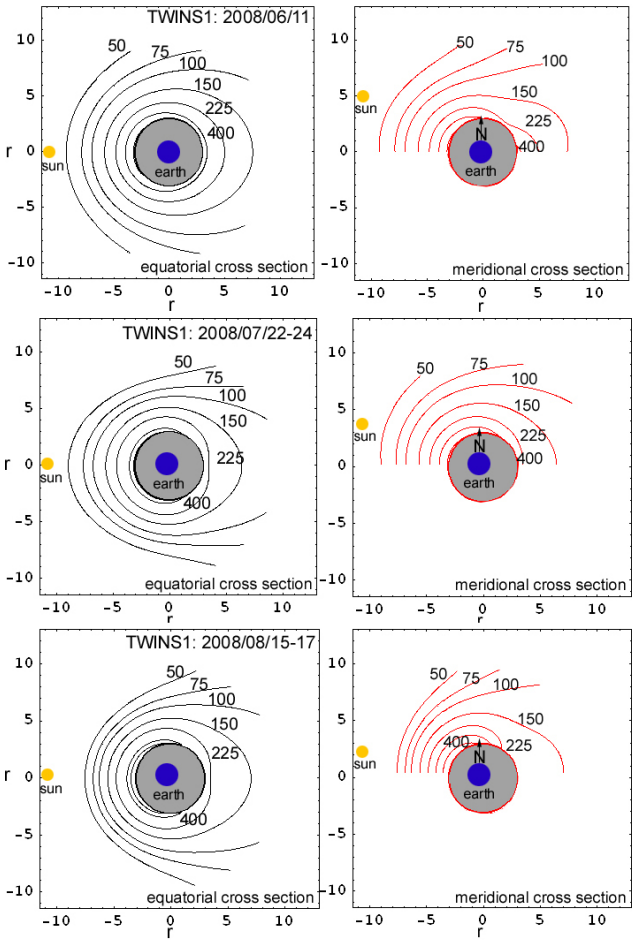

Fig. 6. 3-D-fitted H-density profiles of the geocorona (contours are showing H-density in $\mathrm{cm^{-3}}$) as equatorial cross section (left, black) respectively meridional cross section along the pole axis (right, red) for 3 different dates between June and August 2008. The grey area around the earth shows the optical thick region with geocentric distances $r < 3\,R_{\mathrm{E}}$.

5.3 Fitted density contours

For the three mentioned dates between June and August 2008 we present three-dimensional H-density fits of the geocorona. Figure 6 show in the left column (black lines) H-density contours for an equatorial cross section (i.e. for low latitudes). On the right (red lines) H-density contours for the meridional cross section along the north pole axis are shown (Southern Hemisphere was not observed so far).

The complete 3-D-fit process is separated into two steps: First, solely the N(r)-dependence of the 3-D-model is fitted, in a second step the fit of the angle dependent terms is carried out using the fixed values for the N(r)-term found in step 1. The grey region in Fig. 6 marks the excluded low altitude region for low geocentric distances $r < 3\,R_{\mathrm{E}}$, which is dominated by multiple scattering processes because of the optically thick conditions prevailing here.

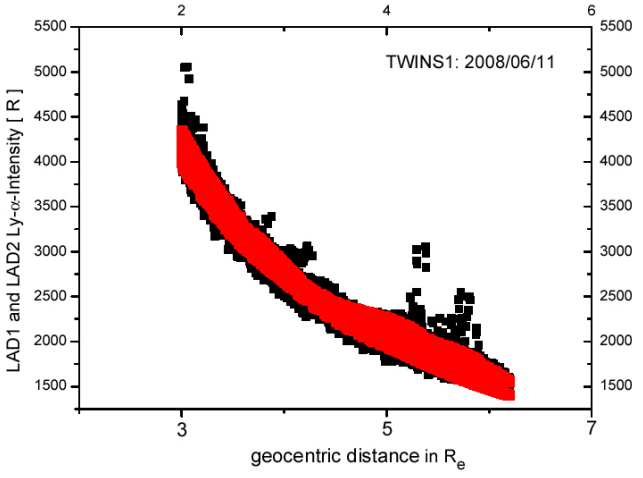

Fig. 7. Measured TWINS Ly-α-intensity profile in Rayleigh (11 June 2008) plotted versus the "line-of-sight" (LOS) earth passing geocentric distance in R_E. The red area is showing the calculated LOS-intensities based on the 3-D r,θ,ϕ-dependent "Bonn"-H-density model which fits the general profile and is able to explain the width of scattering within the profile.

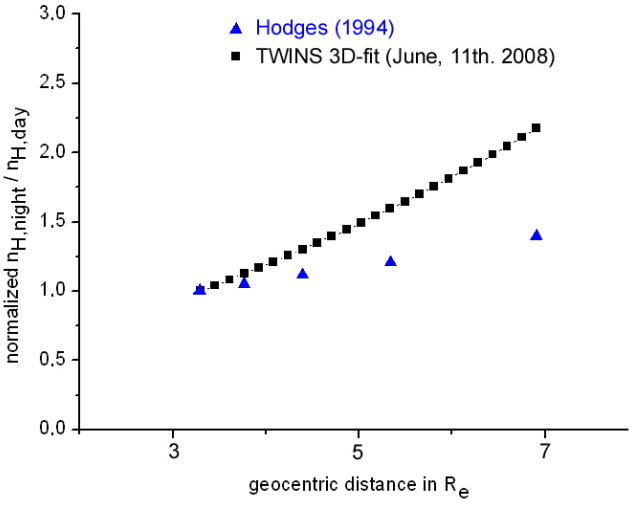

Fig. 8. Day-/nightside normalized H-density ratio (at the equator) as fitted with the 3-D H-density model (black) for 11 June 2008 and compared with the solstice-model (10.7 cm radioflux = 80) by Hodges (1994) (blue). H-densities on both sides were normalized to corresponding reference density values at 3 R_E.

In the equatorial cross section (left) and meridional cross section (right) a clear and remarkable solar/antisolar asymmetry of the H-density is manifest.

In contrast to the simple r-dependent H-density model the fitted 3-D-density model with its angle-dependent terms is able to explain most of the observed TWINS-LAD-1/2 Ly-α-intensity scatters for lines of sight with different view directions but with identical impact altitudes. As seen in Fig. 7 the red area as the result of the 3-D-fitted model intensities is able to explain most of the scattering (as seen in the black area).

5.4 Day-/nightside asymmetry

An obvious, outstanding, and characteristic feature of the H-geocorona fits is the pronounced H-density asymmetry between day- and nightside profiles in the equatorial region. Most probably caused by the solar radiation pressure and the geocoronal H-atom charge exchange interactions with the subsonic post-bow-shock solar wind proton flow the equatorial dayside H-density for geocentric distances $r > 4\ R_E$ seems to be reduced in comparison with corresponding nightside densities.

Compared to the sun-ward side the H-density on the anti-sunward side decreases with altitude much slower indicating clearly a tail-like H-geocoronal structure. At 7 R_E this means that the predicted anisotropy value of the normalized H-density (see Fig. 8) is $\approx 40\%$ lower as reflected by the TWINS-data. The existence of such a geocoronal H-geotail, i.e. the phenomenon of a preferential over-population of H-atom satellite orbits with apogees located on the nightside of the earth had already been recognized much earlier in geocoronal studies by Thomas and Bohlin (1972). A possible process to support the tail-population of the H-geocorona could be seen in a continuous apogee shift of H-atoms in elliptical satellite orbits towards the nightside equatorial region caused by the action of solar (mostly) Ly-α radiation pressure onto these orbiting atoms. The head-to-tail normalized H-density asymmetry observed with TWINS-LAD is much more pronounced than predicted by the H-geocorona model published by Hodges (1994). This asymmetry appears in all of the three H-density 3-D-fits carried out with the TWINS1-data between June and August 2008. In addition, however, the indicated degree of asymmetry between equatorial and polar densities is found to be weaker then expected from the model given by Hodges (1994).

6 Conclusions and comparison with other planetary exospheres

The simple r-dependent H-density profiles of the H-geocorona for geocentric distances of $r < 4.5\ R_E$ presented in the beginning of this paper are in reasonably good agreement both with the results presented by Østgaard and Mende (2003) and with the predictions of the Hodges-model (1994). For larger distances $r > 4.5\ R_E$, however, the TWINS-derived H-density profiles decrease less rapidly than the profiles given in the two before mentioned publications. A possible explanation of this challenging fact is the unexpectedly strong presence of an H-satellite particle component, i.e. a component of H-atoms orbiting the earth in long living Keplerian trajectories with perigees above the exobase (see Chamberlain, 1963). Such satellite-type H-atoms are

likely to dominate in the uppermost regions of the geocorona (see Richter et al., 1979; Fahr and Shizgal, 1983), and with the densities derived from TWINS-LAD data one should feel encouraged to investigate mechanisms to populate these H-atom satellite orbits.

The simple r-dependent H-density model, as we have shown, could furthermore not explain the observed scatter in the data of the LAD-1/2 Ly-α-intensity for lines of sight with identical LOS impact altitudes but different viewing directions. That phenomenon allows to conclude the predominance of pronounced angle-dependent H-density structures established in the geocorona.

The 3-D density fits of the H-geocorona finally presented in this paper clearly reveal a pronounced day-/night-side asymmetry in the equator region. This TWINS-derived asymmetry definitely is stronger than presented in the other two reference density models with which we have compared our data. On the night region of the earth the H-density extends to much larger geocentric distances compared to corresponding dayside densities. This can become understandable as indication of a geotail-like H-density structure at the night side due to H-satellite atoms in elliptical orbits with apogees on the nightside of the earth.

In addition we find that the north pole/equator asymmetry of the H-density observed by TWINS1 is much weaker than given in the Hodges-model (1994). That is a possible hint to the fact that the reduction of the neutral H-density over the poles caused by the charge-exchange coupling between H-exosphere and the polar wind is less effective as taken into account in model calculations by Hodges (1994).With new TWINS-LAD data obtainable in the upcoming time period we can hope to more thoroughly study this interesting phenomenon.

The scattering of the Ly-α-intensity for LOS passing the earth with equal distances but observed from different points of view is satisfactorily well explained by application of our 3-D-model with its angle-dependent terms. Furthermore Ly-α-intensity variations on small time-scales are observed and may be explainable by temporal variations of the upper H-exosphere (see Paul and Fahr, 1979). These phenomena are still an open problem for further investigations.

As judged from a series of other publications, the phenomenon of an unexpectedly wide extent of the planetary H-corona confirmed by our data for the case of the terrestrial H-corona is also manifest at other planets. For instance in Delva et al. (2009) it is reported that Venus has a largely extended hydrogen exosphere with significant local H-densities up to altitudes even beyond eight planetary radii. This became evident from ion cyclotron wave observations made by the Venus Express magnetometer in the solar wind regime near Venus. These waves are due to pick-up protons created by charge exchange of Venusian H-atoms in the near-Venusian solar wind (see e.g. Huddleston and Johnstone, 1992; Huddleston et al., 1997) and can prove the presence of unexpectedly high Venusian H-atom densities at large planetary distances. H-densities extracted from existing models like by Hodges (1994) fall much below these values, and the models obviously require the inclusion of a hot H-atom component like that taken into account by Gunell et al. (2005).

A similar phenomenon of a largely extended H-corona has also been detected with UV spectrometer SPICAM on Mars Express (Chaufray et al., 2007, 2008). A Chamberlain model applied to the Martian H-exosphere obviously fails to correctly fit the extent of the Martian Ly-α corona and a supplementary hydrogen population, perhaps from exothermal chemistry with CO_2- or HCO- Martian ions involved, is definitely needed to reconcile these Martian Ly-α observations. Similar conclusions are drawn by Galli et al. (2006) on the basis of Ly-α limb observations carried out with the ASPERA-3 instrument on Mars Express. Also here the request for a hot Martian H-atom component corresponding to a temperature around 1000 K is formulated.

Acknowledgements. Topical Editor C. Jacobi thanks D. Shemansky and another anonymous referee for their help in evaluating this paper.

References

Barth, C. A., Rottman, G. J., Tobiska, W. K., and White, O. R.: Comparison of 10.7 CM radio flux with SME solar Lyman alpha flux, Geophys. Res. Lett., 17, 571–574, 1990.

Bishop, J.: Analytic exosphere models for geocoronal application, Planet. Space Sci., 39, 885–893, 1991.

Bzowski, M., Mäkinen, T., Kyrölä, E., Summanen, T., and Quémerais, E.: Latitudinal structure and north-south asymmetry of the solar wind from Lyman-alpha remote sensing by SWAN, Astronomy and Astrophysics, 408, 1165–1177, 2003.

Chamberlain, J. W.: Planetary coronae and atmospheric evaporation, Planet. Space Sci., 11, 901–960, 1963.

Chaufray, J. Y., Modolo, R., Leblanc, F., Chanteur, G., Johnson, R. E., and Luhmann, J. G.: Mars solar wind interaction: Formation of the Martian corona and atmospheric loss to space, J. Geophys. Res., 112(E9), E09009, doi:10.1029/2007JE002915, 2007.

Chaufray, J. Y., Bertaux, J. L., Leblanc, F., and Quémerais, E.: Observation of the hydrogen corona with SPICAM on Mars Express, Icarus, 195(2), 598–613, 2008.

Delva, M., Volwerk, M., Mazelle, C., Chaufray, J. Y., Bertaux, J. L., Zhang, T. L., and Vörös, Z.: Hydrogen in the extended Venus exosphere, Geophys. Res. Lett., 36(1), L01203, doi:10.1029/2008GL036164, 2009.

Fahr, H. J.: Global structure of the heliosphere and interaction with the local interstellar medium: three decades of growing knowledge, Adv. Space Res., 34(1), 3–13, 2004.

Fahr, H. J., Fichtner, H., and Scherer, K.: Theoretical aspects of energetic neutral atoms as messengers from distant plasma sites with emphasis on the heliosphere, Rev. Geophys., 45(4), RG4003, 1–38, 2007.

Fahr, H. J. and Shizgal, B.: Modern Exospheric Theories and Their Observational Relevance, Rev. Geophys. Space Phys., 21, 75–124, 1983.

Galli, A., Wurz, P., Lammer, H., Lichtenegger, H. I. M., Lundin, R., Barabash, S., Grigoriev, A., Holmström, M., and Gunell, H.: The

Hydrogen Exospheric Density Profile Measured with ASPERA-3/NPD, Space Sci. Rev., 126(1–4), 447–467, 2006.

Gunell, H., Holmström, M., Biernat, H. K., and Erkaev, N. V.: Planetary ENA Imaging: Venus and a comparison with Mars, Planet. Space Sci., 53(4), 433–441, 2005.

Hodges Jr., R. R.: Monte Carlo simulation of the terrestrial hydrogen exosphere, J. Geophys. Res., 99, 23229–23247, 1994.

Holzer, T. E. and Banks, P. M.: Accidentally resonant charge exchange and ion momentum transfer, Planet. Space Sci., 17, 1074–1077, 1969.

Huddleston, D. E. and Johnstone, A. D.: Relationship between wave energy and free energy from pickup ions in the Comet Halley environment, J. Geophys. Res. (ISSN 0148-0227), 97(A8), 12217–12230, 1992

Huddleston, D. E., Strangeway, R. J., Warnecke, J., Russell, C. T., Kivelson, M. G., and Bagenal, F.: Ion cyclotron waves in the Io torus during the Galileo encounter: Warm plasma dispersion analysis, Geophys. Res. Lett., 24, 2143–2146, 1997.

McComas, D. J., Allegrini, F., Baldonado, J., Blake, B., Brandt, P. C., Burch, J., Clemmons, J., Crain, W., Delapp, D., Demajistre, R., Everett, D., Fahr, H., Friesen, L., Funsten, H., Goldstein, J., Gruntman, M., Harbaugh, R., Harper, R., Henkel, H., Holmlund, C., Lay, G., Mabry, D., Mitchell, D., Nass, U., Pollock, C., Pope, S., Reno, M., Ritzau, S., Roelof, E., Scime, E., Sivjee, M., Skoug, R., Sotirelis, T. S., Thomsen, M., Urdiales, C., Valek, P., Viherkanto, K., Weidner, S., Ylikorpi, T., Young, M., and Zoennchen, J. H.: The Two Wide-angle Imaging Neutral-atom Spectrometers (TWINS) NASA Mission-of-Opportunity, Space Sci. Rev., 142(1–4), 157–231, 2009.

Nass, H. U., Zoennchen, J. H., Lay, G., and Fahr, H. J.: The TWINS-LAD mission: Observations of terrestrial Lyman-α fluxes, Astrophys. Space Sci. Trans., 2, 27–31, doi:10.5194/astra-2-27-2006, 2006.

Østgaard, N., Mende, S. B., Frey, H. U., Gladstone, G. R., and Lauche, H.: Neutral hydrogen density profiles derived from geocoronal imaging, J. Geophys. Res. Space Phys., 108(A7), 18-1, 2003.

Paul, G. and Fahr, H. J.: Propagation of the geomagnetic density and temperature effect into the exosphere, Planet. Space Sci., 27, 403–409, 1979.

Pryor, W., Gangopadhyay, P., Sandel, B., Forrester, T., Quémerais, E., Möbius, E., Esposito, L., Stewart, I., McClintock, W., Jouchoux, A., Colwell, J., Izmodenov, V., Malama, Y., Tobiska, K., Shemansky, D., Ajello, J., Hansen, C., and Bzowski, M.: Radiation transport of heliospheric Lyman-a from combined Cassini and Voyager data sets, Astron. Astrophys., 491(1), 21–28, 2008.

Richter, E., Fahr, H. J., and Nass, H. U.: Satellite particle exospheres of planets – Application to earth, Planet. Space Sci., 27, 1163–1173, 1979.

Richter, M., Kroth, U., Thornagel, R., Fahr, H. J., Lay, G., and Nass, H. U.: Calibration of Lyman-α detectors for the NASA satellites TWINS, BESSY Annual Report 2001, S. 15, 2001.

Thomas, G. E. and Bohlin, R. C.: Lyman-alpha measurements of neutral hydrogen in the outer geocorona and in interplanetary space., J. Geophys. Res., 77, 2752–2761, 1972.

Vidal-Madjar, A.: Evolution of the solar Lyman alpha flux during four consecutive years, Solar Phys., 40, 69–86, 1975.

Wu, F. M. and Judge, D. L.: Temperature and flow velocity of the interplanetary gases along solar radii, Astrophys. J., Part 1, 231, 594–605, 1979

Zoennchen, J. H.: Modellierung der dreidimensionalen Dichteverteilung des geokoronalen Neutralwasserstoffes auf Basis von TWINS Ly-Alpha-Intensitaetsmessungen, Phd thesis, URN: urn:nbn:de:hbz:5N-08886, URL: http://www.ulb.uni-bonn.de/, 2006.